Lab on a Chip

PAPER

View Article Online
View Journal | View Issue

Cite this: *Lab Chip*, 2014, **14**, 342

Resolution enhancement of suspended microchannel resonators for weighing of biomolecular complexes in solution†

Mario M. Modena, Yu Wang, Dietmar Riedel and Thomas P. Burg*

Received 17th September 2013,
Accepted 28th October 2013

DOI: 10.1039/c3lc51058a

www.rsc.org/loc

We introduce the use of correlation analysis to extend the dynamic range of suspended micro- and nanochannel resonator (SMR/SNR) mass sensors by over five orders of magnitude. This method can analyze populations of particles flowing through an embedded channel micromechanical resonator, even when the individual particle masses are far below the noise floor. To characterize the method, we measured the mass of polystyrene nanoparticles with 300 zg resolution. As an application, we monitored the time course of insulin amyloid formation from pre-fibrillar aggregates to mature fibrils of 15 MDa average mass. Results were compared with thioflavin-T (ThT) assays and electron microscopy (EM). Mass measurements offer additional information over ThT during the fluorescent inaccessible lag period, and the average fibril dimensions calculated from the mass signal are in good accordance with EM. In the future, we envision that more detailed modeling will allow the computational deconvolution of multicomponent samples, enabling the mass spectrometric characterization of a variety of biomolecular complexes, small organelles, and nanoparticles in solution.

Introduction

Nanomechanical resonators have received considerable attention for applications ranging from the study of quantum mechanical effects to biotechnology.[1–7] The high quality factors (Q) and the small sizes of such resonators have recently permitted measurement of mass with yoctogram resolution (1 yg = 10^{-24} g),[8] and NEMS (Nanoelectromechanical Systems) based mass spectrometry under vacuum has already been demonstrated.[9] However, translating the highest levels of sensitivity attained under vacuum conditions to the solution environment of biological molecules is a non-trivial task. In addition to the fundamental degradation in sensitivity due to fluid viscosity, there are many practical challenges associated with the operation of ultra-small nanomechanical resonators in aqueous buffers. With the introduction of suspended micro- and nanochannel resonators[10–13] (SMRs and SNRs), it has become possible to measure the buoyant mass of particles in solution with a resolution on the 10 ag scale. Measurements in flow-through mode (without surface functionalization) have been able to detect single nanoparticles weighing less than 100 ag[13] and similar devices have been used to characterize single cell densities[14–16] and coatings on microparticle surfaces.[17]

Max Planck Institute for Biophysical Chemistry, Göttingen, Germany. E-mail: tburg@mpibpc.mpg.de

† Electronic supplementary information (ESI) available: Detailed description of the fit function; calibration information; supporting measurements and EM images of the reported data. See DOI: 10.1039/c3lc51058a

Despite great efforts to further improve the sensitivity of embedded channel resonators by direct miniaturization,[11,13] there are two significant challenges on this path yet to be addressed. One is the need to maintain frequency resolution in the parts-per-billion range with resonators scaled to sub-micrometer dimensions. Continuous progress in this area is made through the optimization of device technology and readout techniques. A more fundamental problem, however, is posed by the diminishing rate of single-particle detection events at a given solution concentration as the device size is reduced. Studies by Arlett and Roukes[18] suggest that this may set a practical limit on the resolution of embedded channel resonators near the one attogram (10^{-18} g) mark, independent of further miniaturization. Large-scale integration of nanoelectromechanical systems may partially address this challenge by providing vast arrays of sensors with on-chip electronics. However, this route is technologically complex and may only be viable for specific device types.

The important trade-off between sensitivity and sample throughput in embedded channel resonators is intimately linked to the requirement for the reliable detection of individual particles: a reduction in bandwidth improves the detection limit at the expense of lowering the event count rate for a given sample concentration. This ultimately limits the statistics, since single-particle detection requires the concentration to always be below approximately one particle per detector volume. The strict requirements of single-particle detection have so far precluded all applications of embedded

channel nanomechanical resonators to problems involving nanoparticles, small organelles, or macromolecular complexes in the sub-100 MDa range.

Here we introduce the concept of correlation analysis of the time-domain mass signal to extend the measurement range of embedded channel resonators into the regime where individual particle signatures cannot be distinguished. Correlation analyses have found wide applications for improving signal-to-noise ratio in the study of stochastic events lying in a noisy background.[19–22] However, the technique so far has never been applied in the context of nanomechanical mass measurements in liquid.

To illustrate one possible application, we use resolution enhancement to monitor the growth kinetics of amyloid fibrils in solution by mass, starting from pre-fibrillar aggregates to mature fibrils. The conversion of soluble proteins into amyloid fibrils has been associated with over 40 human diseases, such as Alzheimer's, Parkinson's or type II diabetes,[23,24] and quantitative measurements of this process are thus of great interest. Furthermore, protein aggregation often presents a challenge in biotechnology and pharmaceutical formulations, where unwanted protein degradation can occur during production, purification, handling and storage.[25,26] Our technique provides a unique new tool to study such processes, as the mass signal is complementary to the information obtained by conventional methods, including light scattering, fluorescence, or X-ray diffraction.[27] An important difference to measurements obtained using the quartz crystal microbalance (QCM), surface plasmon resonance (SPR), and microcantilever stress sensors is that no surface attachment of the molecules is required.[28]

Theory

When a particle flows through the inside of a suspended microchannel resonator, it produces a transient shift in the resonance frequency (Fig. 1). This effect is caused by the particle excess mass Δm with respect to the fluid in which it is suspended.[10,13] The magnitude of the frequency shift induced at any specific axial position is proportional to the

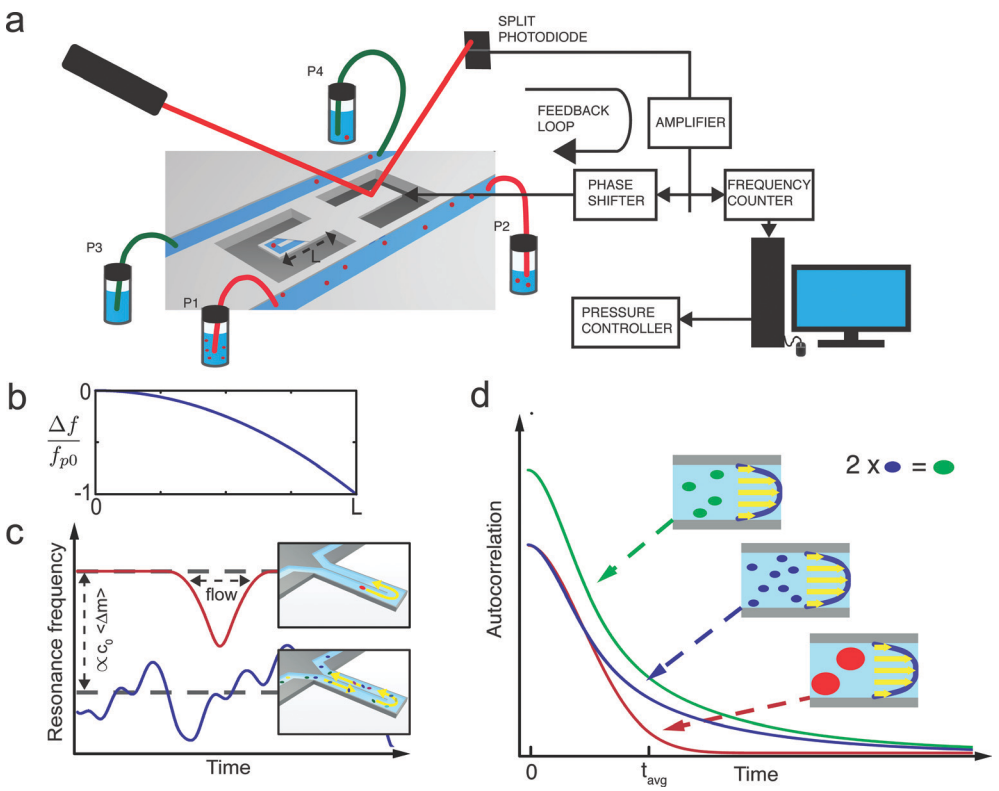

Fig. 1 a) Experimental setup for the suspended microchannel resonator comprising a torsional microresonator with embedded microfluidic channels (3 × 8 μm cross section), an optical lever system to detect the oscillation, and a feedback loop for exciting the resonance vibration. Pressurized fluid reservoirs are used to accurately control the flow in the microfluidic channels. b) The sensitivity profile for loading by a point mass is approximated as a parabolic function of position. The frequency shift reaches a maximum when the particle is at the apex of the resonator. c) When a single particle flows through the resonator, the resonance frequency signal exhibits a characteristic peak (red curve). The shape of the peak is a function of the sensitivity profile and of the flow velocity. When many particles travel through the resonator at the same time, their effects add linearly to cause a shift in the baseline and additional fluctuations. d) Expected autocorrelation curves of time domain mass signals as a function of sample composition: in red, autocorrelation for a sample composed of particles whose diameter is similar to the channel size. In blue, long-tailed autocorrelation for small particles, which are able to sample the slower parts of the velocity profile. As the mass of the particles increases (green curve), the autocorrelation maximum grows, even when the total dissolved mass is kept constant. The autocorrelation amplitude depends solely on sample concentration and sample mass, while the autocorrelation shape varies with the particle dimension.

square of the local vibration amplitude $u(x)$ of the resonator at this location.[29] In the case of cantilever resonators vibrating in the fundamental mode, the frequency shift reaches a maximum when the particle is at the apex of the cantilever.

When particles in the sample are present at a high concentration, they alter the effective mass density of the solution, leading to a shift in the mean value of the resonance frequency. However, this shift is difficult to measure with precision, since slow varying offsets, such as thermal drift or nonspecific binding, tend to overwhelm the effect in practical experiments.

Instead of looking at static shifts in resonance frequency, here we focus on the number density fluctuations of discrete particles randomly dispersed in the flowing liquid. These induce fluctuations in the resonance signal *via* the linear superposition of varying numbers of individual single-particle signatures. Interestingly, white noise in the measurement can be largely separated from these particle number fluctuations by analyzing the autocorrelation‡

$$C(\tau) = \langle \delta f(t) \delta f(t + \tau) \rangle \quad (1)$$

of the resonance frequency fluctuations δf. Brackets '$\langle \bullet \rangle$' represent the ensemble-based expected value, and δf is the high-pass filtered signal having zero mean and no baseline drift. The effect of white noise in δf on $C(\tau)$ is strongly confined to values of $\tau \approx 0$, while frequency fluctuations due to passing particles affect $C(\tau)$ at $\tau > 0$. The magnitude of $C(\tau)$ carries information about the mass and concentration of the particles, while information about their size, diffusivity, and interactions with each other and with the flow profile affects the shape of the function. Although modeling all of these effects analytically in the geometry of the SMR is mathematically complex, we now show that a simple compartment model fits the measurements with high accuracy in many important practical cases. The model divides the channel cross section into M compartments of area A_i ($i = 1 \ldots M$), inside of which the flow profile is approximated as a plug flow of velocity v_i. The analytical autocorrelation for each compartment is readily evaluated (see ESI†):

$$C_i(\tau) = {f_{p0}}^2 \, c_0 A_i \, g(v_i \, \tau), \quad (2)$$

with f_{p0} the frequency shift induced by a single particle, c_0 the average sample concentration, and $g(s) = \int u(x)^2 u(x - s)^2 \mathrm{d}x$ given in the ESI.† Choosing an appropriate number and size A_i (area) of the compartments enables the model to partially account for effects of finite particle size and diffusion. To illustrate this, we first consider particles whose size is comparable to the channel cross section. Such particles are unable to closely approach the wall and thus exhibit a relatively narrow velocity distribution. Therefore, a single compartment with an associated velocity equal to the mean flow velocity of the fluid is adequate for describing the signal. In contrast, smaller particles travel at different velocities according to their position in the channel cross section.[30] An appropriate choice for the size of the compartments is given by the characteristic distance particles able to diffuse during their passage through the resonator. To analyze real measurements, we employ the complete normalized autocorrelation

$$G(\tau) = \frac{\sum_{i=1}^{M} C_i(\tau)}{\sum_{i=1}^{M} C_i(0)} \quad (3)$$

as the basis for a two-parameter model, $\beta_1 G\left(\beta_2 \frac{k}{f_s}\right)$, which is used to fit the sample autocorrelation

$$\hat{C}[k] = \frac{1}{N-k} \sum_{i=1}^{N-k} \delta f_i \bullet \delta f_{i+k} \quad (4)$$

Here δf_i denotes the sampled and AC-filtered signal ($i = 1 \ldots N$; $N = [T_{meas} \cdot f_s]$; f_s = sampling rate). The extracted parameter $\hat{\beta}_1$ represents the magnitude of the signal and has the expected value $\left\langle \hat{\beta}_1 \right\rangle = \frac{1}{5} {f_p}^2 c_0 V$, where V is the volume of the resonator. The timescale $\hat{\beta}_2$ is related to the average passage time of the particles and therefore provides information about the flow velocity. Note that for heterogeneous samples, ${f_{p0}}^2$ in the above analysis would be replaced by a population average.

Materials and methods

Suspended microchannel resonators

A torsional SMR device shown schematically in Fig. 1 was used for the polystyrene and insulin measurements. The same chip was used in all experiments. The fabrication has been described previously[10] and we therefore only summarize the key steps here: channels having a nominal depth of 3 μm were etched into silicon and sealed using fusion bonding to another silicon wafer. The resonator was subsequently defined by dry etching and vacuum packaged by bonding to two Pyrex wafers, one of which provided electrostatic actuation electrodes and a getter layer for maintaining a stable on-chip vacuum. Fluidic connections were made using flanged FEP tubing attached to the surface of the chip.

The outer dimensions of each of the two paddles of the resonator were designed as 60 μm × 36 μm × 7 μm (length × width × thickness). Each of the paddles contained a U-shaped channel with a cross-sectional area of 8 μm × 3 μm.

Under gas flow, the resonator presented a resonance frequency of 1.17 MHz and a quality factor of ~23 000. When filled with liquid, the resonator experienced a reduction of the quality factor to ~6000 and a 200 mHz frequency stability in a 1 kHz bandwidth. The oscillation of the SMR was detected

‡ In statistics, the function $C(\tau)$ is known as 'autocovariance', but in other fields it is often called 'autocorrelation' with varying normalization. For clarity, we always use the word 'autocorrelation' to refer to $C(\tau)$, and otherwise explicitly write 'normalized autocorrelation', mentioning the scale factor.

by an optical lever, and resonance oscillation was ensured by using an oscillator circuit.[31]

Pressurized inlets and outlets allowed accurate control and stability of the fluid flow conditions during measurements, providing a smooth, pulse-free flow through the resonator at rates on the scale of 100 pL s^{-1}. To maximize the stability of the resonance frequency, the resonator was placed on a temperature controlled stage. All measurements were performed at 25 °C.

Cleaning of the device in case of clogging was accomplished by flowing approximately 10 μL of a mixture of sulfuric acid and hydrogen peroxide (piranha solution) through the bypass channels. This also forced some of the solution into and through the resonator, such that the device was thoroughly cleaned and could be re-used numerous times. To avoid corrosion of the external fluidics and connections, only FEP tubing directly fitted to the silicon/glass SMR chip was used in this procedure.

Polystyrene bead measurements

85 nm polystyrene beads (2.6% w/v stock solution, Polysciences, Inc. lot# 621931) were suspended in an aqueous buffer containing 100 mM NaCl, 350 μM SDS and 0.01% w/v NaN_3, at different final concentrations to ensure the consistency of the measurement. The purpose of detergent (SDS) in the buffer was to minimize the risk of clogging due to particles sticking to each other or to the channel walls. The final concentrations were 7.57×10^{12} and 1.15×10^{13} per mL^{-1} (0.25% w/v and 0.38% w/v, respectively). These values were calculated considering a polystyrene density of 1.05 g cm^{-3} and bead dimension, as reported by the manufacturer. All samples were then mixed with 1.54 μm NIST polystyrene particles (Polysciences, Inc. lot# 611330) diluted to yield a final concentration of 5×10^6 per mL^{-1}. Mass measurements with the SMR were performed in 750 Hz and 1 kHz bandwidths.

Insulin aggregation

5 mg mL^{-1} recombinant human insulin (Sigma-Aldrich) was dissolved in 50 mM glycine (Calbiochem) adjusted with HCl to obtain a final pH value of 2.3. To remove amorphous aggregates that might act as aggregation centers, the solution was centrifuged at 30 000 × *g* at 4 °C for 45 minutes. Then, the supernatant was collected and filtered with a 0.22 μm filter. 1 mL of this solution was stirred in a glass vial with a magnetic bead at 37 °C, to promote protein aggregation and fibril formation.[32]

For measurements with the SMR, aliquots of 75 μL of the incubated insulin solution were mixed with 1.54 μm NIST polystyrene particles (Polysciences, Inc. lot# 611330) diluted to yield a final concentration of 5.5×10^6 beads mL^{-1}. Mass measurements of each aliquot were performed in 500 Hz and 1 kHz bandwidths.

Thioflavin-T (ThT) assay

ThT (Sigma Aldrich) was dissolved in 50 mM glycine, pH = 8.2, at a concentration of 500 μM and stored at 4 °C. At each time point, 3 μL aliquots of the incubated sample were added to 87 μL of ThT solution and mixed properly before measuring the fluorescence emission with a NanoDrop 3300 (Thermo Scientific) fluorospectrometer. Excitation and emission wavelengths were, respectively, 470 nm and 506 nm. Ultrapure Milli-Q water was used for blank measurements. For each time point, three repetitions were performed and the average emission value considered. The error bars in Fig. 4 and 5 show the difference between the maximum and the minimum value recorded per time point. The fluorescence measurements were performed at room temperature.

Results and discussion

To demonstrate the enhancement in dynamic range of suspended microchannel resonators, we measured a mixture of polystyrene beads of 85 nm and 1.54 μm diameter. As shown in the inset in Fig. 2, the frequency shift induced by single 1.54 μm particles is significantly greater than the noise

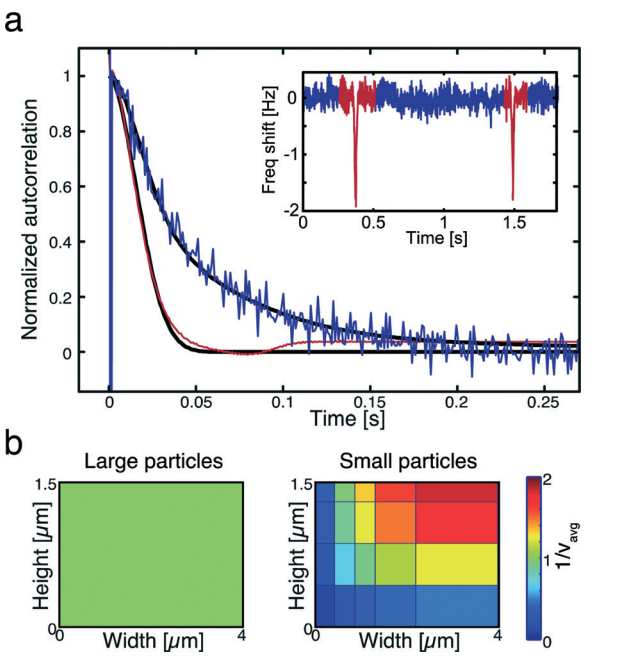

Fig. 2 Normalized autocorrelations for 85 nm polystyrene beads (blue) and 1.54 μm polystyrene reference particles (red) measured as a mixed sample. In black, the functions used to fit the experimental curves. For the larger particles, a single velocity fit accurately describes the experimental data. The smaller particles, instead, show a wider velocity distribution and a compartment model fit has to be used. A short excerpt of the filtered time domain trace is shown in the inset, highlighting the 1.54 μm bead contribution (in red) and the part of the signal used for calculating the 85 nm signal (blue). Both autocorrelation signals are normalized to their maximum for comparison. b) Graphical representation of the velocity streams in the cross section considered for calculating the fit function. On the left, the large particle case, where all particles travel at the average velocity. On the right, the cross section partitioning to account for a wider velocity distribution. Velocity normalization is done according to the average flow velocity, V_{avg}. Only one quarter of the channel cross section is displayed due to symmetry.

(red). However, the mass of the 85 nm beads is nearly 6000 times smaller, and individual particles cannot be detected. By computationally separating all large peaks from the remaining featureless intervals (blue), the data was grouped into two categories, for which the sample autocorrelations were then calculated. The autocorrelation obtained from the signal between large peaks clearly reveals the presence of the small particles. Interestingly, the shape of the autocorrelation is markedly different when calculated from the sections containing large peaks. This can be explained by the difference in diameter. Small particles experience a large dispersion in flow velocity, since they are distributed throughout the entire cross-section of the resonator. In contrast, the larger particles possess a diameter similar to the channel height and are restricted in their ability to sample the velocity profile. They thus travel at a more uniform velocity and the autocorrelation drops to zero at short lag times. The effect of finite particle size is taken into account in the model *via* the discretization of the flow profile, as shown in Fig. 2b.

The magnitude of the sample autocorrelation scales with particle concentration, as shown in Fig. 3a. The recorded time-domain trace has a frequency noise level of ~200 mHz in a 1 kHz bandwidth, which translates into a single-particle detection limit of ~30 fg at a signal-to-noise ratio of 3. Using correlation analysis we were able to obtain a signal-to-noise ratio of ~50 for the autocorrelation curve by measuring 20 nL of sample in less than 3 minutes (average particle transit time ~50 ms). This noise level corresponds to a 300 zg statistical error in the estimation of the mean buoyant mass of the particles. As negative control, we measured a sample of pure buffer solution under the same conditions. As expected, the autocorrelation is flat, except for the points of maximum noise intensity at $\tau \approx 0$ (Fig. 3a). These measurements have been repeated under different flowing conditions, to ensure the reproducibility and the consistency of the results (see ESI†). Knowing the sample concentration, we found that a single polystyrene nanoparticle in the test sample on average induces a frequency shift of −467 ± 16 μHz. According to the mass responsivity calculated from the reference particles (see ESI†), this corresponds to a mean buoyant mass of 21.5 ± 0.7 ag (reproducibility error), or a diameter of 97 ± 1 nm. The mean diameter is in agreement with the manufacturer specifications of 85.4 ± 6.5 nm considering systematic uncertainties in calibration, for example due to manufacturing tolerances in the device geometry.

Although the spread between different devices was not analyzed in this study, a bound of approximately ±1 μm can be placed on the manufacturing tolerance in the channel depth. This would result in a 30% uncertainty in channel volume, corresponding to approximately 5% systematic uncertainty when estimating the average particle diameter.

How far the detection limit of suspended micro- and nanochannel resonators can be enhanced by correlation analysis can be estimated by calculating the signal-to-noise ratio (S/N ratio) as a function of concentration and measurement time. This is approximated as the magnitude of the

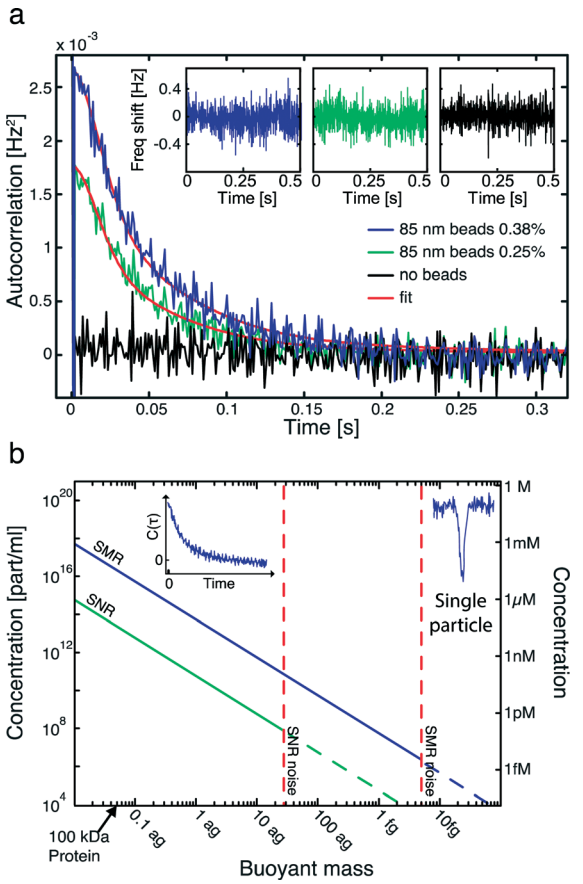

Fig. 3 a) Autocorrelation functions for a sample of 85 nm polystyrene particles at concentrations of 1.15 × 10^{13} parts mL^{-1} (0.38% w/v) and 7.67 × 10^{12} parts mL^{-1} (0.25% w/v). As the sample concentration decreases, the autocorrelation maximum is reduced accordingly. In red, the fit function used for amplitude and transit time estimation. The autocorrelation of pure buffer (in black) is shown as negative control. Short excerpts of the 1 Hz high-pass filtered time domain signals are displayed in the insets for comparison. b) Single particle and correlation analysis resolution limits for the double paddle SMR and for suspended nanochannel resonators (SNR). The red dashed lines represent the resolution limit for the SMR and the SNR in a 1 kHz measurement bandwidth. The blue and green lines show the minimum required concentration for having a signal-to-noise ratio = 1 when analyzing the correlation functions, using the SMR and the SNR respectively. The curves shown here are calculated considering σ_n = 5 fg for the SMR and σ_n = 27 ag for the SNR and T_{meas} = 200 s.

autocorrelation divided by the residual noise in $\hat{C}[k]$, which has variance $\sigma_{\hat{C}}^2 \approx \frac{\sigma_n^4}{N}$ $(0 < k \ll N)$:

$$\mathrm{S/N} \geq \frac{1}{5}\frac{{f_{p0}}^2}{{\sigma_n}^2} c_0 V \sqrt{T_{meas} f_s} \qquad (5)$$

Here ${\sigma_n}^2$ denotes the variance of the readout noise, which will depend on the sampling rate f_s for an adequately band limited signal. Fig. 3b shows the minimum concentration required to detect the presence of particles of a given mass

for devices of different size. Eqn (5) shows that the minimum required concentration to obtain a given signal-to-noise ratio scales quadratically with the particle buoyant mass. Furthermore, the signal-to-noise ratio improves with the square root of the measurement time, *i.e.* the time over which data is collected in the experiment.

Importantly, the analysis does not require DC stability of the signal, as only the fluctuations are taken into account. For example, slow drifts in the mass signal, which can arise due to surface adsorption, are removed by the highpass filter before the autocorrelation. Consequently, fluctuation analysis is primarily sensitive to particles that are free to move with the bulk flow, making the results largely independent of the physical and chemical properties of the solid–liquid interface.

Eqn (5) further reveals that shrinking the internal volume effectively reduces the signal-to-noise ratio due to the dependence of S/N on V. However, this reduction would be compensated by the increase in mass responsivity and lower fluid damping (higher Q) in resonators of smaller dimensions.[33] SNRs with mass responsivities 100 times higher than the one employed here have already been demonstrated[13] and our estimates indicate that such devices could potentially achieve zeptogram resolution when measuring samples at mM concentration (green curve in Fig. 3b).

We now describe the application of resolution enhancement by correlation analysis to the direct measurement of insulin aggregation in solution. Insulin aggregates occur as a side effect during subcutaneous treatment of patients affected by diabetes,[34] but these aggregates can also be promoted *in vitro* by exposing the protein to harsh conditions, such as high concentration, acid environments and high temperatures.[32,35,36] Here we show that the resolution enhancement by correlation analysis allows a label-independent measure of protein aggregation with suspended microchannel resonators, with the potential of detecting in the currently inaccessible lag-phase of amyloid formation.[37] We monitored the aggregation process of a sample of 5 mg mL^{-1} recombinant human insulin in 50 mM glycine–HCl at different time points by looking at the fluorescence emission of thioflavin-T (ThT), a common indicator of the presence of fibrils in solution.[38] At the same time points, we also analyzed the insulin solution with our correlation method (Fig. 4). As the total amount of protein in the sample does not vary during the aggregation reaction, the increase in autocorrelation amplitude reflects an increase in aggregate mass and concentration in the solution (Fig. 4a). The time evolution of the ThT signal is typical of nucleation–polymerization processes, showing a clear initial lag phase where the fibril nuclei are formed[37] (Fig. 4b). In contrast, the autocorrelation amplitude provides a direct mass-based representation of the aggregation. By normalizing the autocorrelation amplitude with the total amount of protein in the sample, one obtains the average $\frac{\langle \Delta m^2 \rangle}{\langle \Delta m \rangle}$, which for homogeneous samples converges to the single-particle buoyant mass. Here $\langle \Delta m^2 \rangle$ represents the population-averaged mean square buoyant mass and $\langle \Delta m \rangle$ the population-averaged mean buoyant mass. Fig. 4b shows the increase of the average mass when compared to the ThT intensity. As the autocorrelation signal increases during the ThT blind phase, this is an indicator of the growth of pre-fibrillar aggregates prior to the assembly of amyloid fibrils. Small oligomers are known to occur during amyloid formation,[25,39] and these species are of particular interest due to their putative significance in numerous amyloid associated diseases. The ThT lag phase is inherent to the binding mechanism of the fluorescent dye to the fibrillar

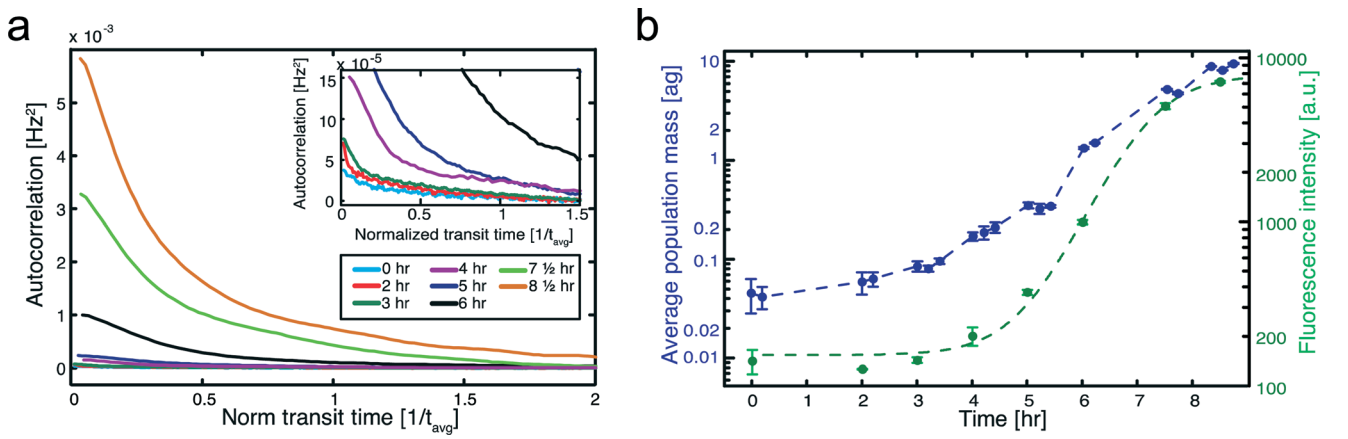

Fig. 4 a) Autocorrelation signals acquired at different time points during insulin aggregation. As the aggregation proceeds, a clear increase in the amplitude is visible, showing growth in the aggregate size and/or concentration. Transit times have been normalized to the average value found with the fit function (fit parameters are reported in the ESI†). The curves have been smoothed with a triangular smoothing over 5 points for clarity. b) Comparison between the growth of the average aggregate mass (in blue) and ThT fluorescence (in green). The ThT fluorescence data are fitted with a sigmoidal, showing the typical nucleation–elongation behavior, with a lag phase of ~3.5 hours. The mass correlation analysis shows a clear increasing trend in average buoyant mass of the aggregates during the lag phase, an indication of the formation of protofibrils in solution. The error bars represent the statistical errors on the fit estimations for each measurement. For the ThT measurements, the error bars are the difference between the maximum and minimum intensity values recorded at each time point.

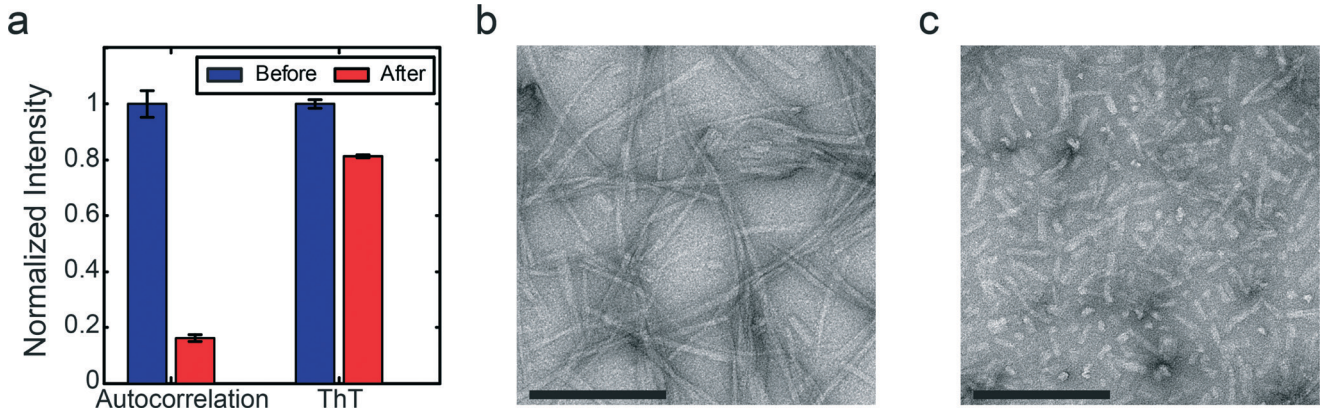

Fig. 5 a) Normalized values for the autocorrelation amplitude and ThT fluorescence intensity of aggregated insulin samples before and after ultrasonication. The values were normalized to their maximum to compare the relative intensity variation. ThT intensity shows a minor reduction, as sonication only causes fibril fragmentation, but not a major diminution in the amount of fibrillated material. On the contrary, the correlation analysis shows a major change in intensity, as the mean mass of the aggregates has been strongly reduced by ultrasonication. b) EM image taken from the same sample before sonication (scale bar 200 nm). c) EM image taken after sonication (scale bar 200 nm). The images confirm the MCS measurement of a strong reduction in fibril length upon ultrasonication.

material, for the binding requires a minimum of four aromatic–hydrophobic cross-strand residues.[38] Absence of a fluorescence signal in this phase thus does not accurately reflect the actual kinetics of amyloid formation. In contrast, by looking at the correlation amplitude of the mass signal, a lag phase would be related to the extremely low buoyant masses of the first products in the aggregation process. Because of the low expected buoyant mass for insulin, detection of monomers (~0.01 ag) in solution would require concentrations approaching 1 M in order to produce a large enough correlation maximum with the SMR used in this work. Therefore, the non-zero autocorrelation intensity at the first time point indicates the presence of small oligomers in solution, but their mass and concentration are not sufficient to obtain a significant signal to noise ratio. After 2 hours of incubation, the aggregates caused strong enough frequency fluctuations that could be analyzed more reliably by the autocorrelation analysis. As such, a resonator with higher mass responsivity could dramatically shorten this blind phase, providing information on the very early steps in the aggregation process.

Another important feature of the mass signal correlation analysis for the characterization of protein aggregates is revealed by observing the difference in signals between freshly formed and ultrasonically fragmented amyloid fibrils. Ultrasonication of amyloid fibrils is a common technique used for preparing seeds from pre-formed fibrils[40,41] or to generate a relatively monodisperse population of fibrils.[42,43] We subjected the 8 1/2 h aggregated sample to two cycles of 15-minute ultrasonication, which was carried out in an ice-water bath to avoid unwanted temperature induced fibril growth. The sonicated sample was then analyzed both by mass and ThT fluorescence measurements. By comparing the results with the non-sonicated sample (Fig. 5a), the ThT intensity shows a 20% decrease in fluorescence, possibly due to a slight reduction in fibrillated material in solution; however, when measured with the SMR, the autocorrelation magnitude of the sonicated sample is reduced by over 80%, revealing a drastic decrease in fibril size. We found an average buoyant mass value of 8.6 ± 0.6 ag (25.2 ± 2.0 ag dry mass) for the non-sonicated sample, and 1.40 ± 0.16 ag (4.2 ± 0.4 ag dry mass) for the sonicated one. Insulin fibrils have an expected mass per length of 2.47 kDa $Å^{-1}$,[44] and the measured mean masses correspond to an expected length of 616 ± 48 nm for the non-sonicated case and 100 ± 8 nm for the sonicated one. These values are in good accordance with the sizes of the fibrils in the EM micrographs for the two samples (Fig. 5b and c, more EM images in the ESI†). Furthermore, since the autocorrelation intensity is the product of mean square mass and particle concentration, it is possible to express a mean fibril concentration, related to the mean aggregate masses reported before. We found an average concentration of 330 ± 50 nM for the non-sonicated sample and 2.0 ± 0.3 μM for the sonicated case.

Conclusions

Correlation analysis of the time-domain mass signal has been proven as a valid method to significantly extend the range of applicability of SMR and SNR devices in flow-through mode. The analysis does not require any specific labeling of the sample or surface functionalization. Importantly, the method makes it possible to detect the presence of discrete particles in solution even when single-particle signals are several orders of magnitude smaller than the readout noise. As shown, the sensitivity can be continuously improved by increasing the measurement time, *i.e.* acquiring more samples at a fixed sampling rate. However, doing this does pose a limit to the time resolution obtainable when studying changing samples, such as, for example, particles undergoing association or dissociation after a step change in solution conditions. In the future, there are two potential routes to

circumvent this limitation. First, a steady-state could be established by placing the bypass channel feeding the resonator in series with a continuous flow mixer. Adjusting the delay between mixer and resonator would thereby enable the characterization of reaction products at specific time points, and time resolution would ultimately be limited by the particle residence time in the resonator. The second route would be applicable for the characterization of reactions that are faster than the residence time. In principle, this is possibly due to the subtle dependence of the shape of the autocorrelation function on the effective diffusivity of interacting particles. However, a more accurate theory would be required to evaluate the feasibility of this in real experiments using mass signals alone.

When the total dissolved mass in solution or the sample concentration are known, our method provides estimates of the average mass of the particles lying below the measurement noise with high accuracy. However, population distribution information cannot be inferred by the current analysis, as the particle contributions in the autocorrelation extend to similar time scales and a decomposition into different population contributions is not possible. We foresee that this restriction can be significantly relaxed by including a more extensive description of particle diffusion in the model describing the autocorrelation function. As shown, particles of diverse sizes sample the laminar flow profile to different extents, and particle diffusion directly affects the residence time distribution of particles in the resonator. By including these effects in the autocorrelation fitting function, particle diffusion could in principle be assessed, enabling a complete label-free population characterization in solution.

Acknowledgements

Suspended microchannel resonator devices were generously provided by the laboratory of Prof. Scott Manalis (MIT, Cambridge, MA). This work was funded by the Göttingen Graduate School for Neurosciences, Biophysics, and Molecular Biosciences, the Max Planck Society, and the Max Planck Institute for Biophysical Chemistry.

References

1 H. G. Craighead, *Science*, 2000, **290**, 1532–1535.
2 M. D. LaHaye, O. Buu, B. Camarota and K. C. Schwab, *Science*, 2004, **304**, 74–77.
3 J. S. Bunch, A. M. Zande, S. S. van der Verbridge, I. W. Frank, D. M. Tanenbaum, J. M. Parpia, H. G. Craighead and P. L. McEuen, *Science*, 2007, **315**, 490–493.
4 K. Jensen, K. Kim and A. Zettl, *Nat. Nanotechnol.*, 2008, **3**, 533–537.
5 Y. T. Yang, C. Callegari, X. L. Feng and M. L. Roukes, *Nano Lett.*, 2011, **11**, 1753–1759.
6 S. Salomon, T. Leïchlé, D. Dezest, F. Seichepine, S. Guillon, C. Thibault, C. Vieu and L. Nicu, *Nanotechnology*, 2012, **23**, 495501.
7 P. S. Waggoner, C. P. Tan and H. G. Craighead, *Sens. Actuators, B*, 2010, **150**, 550–555.
8 J. Chaste, A. Eichler, J. Moser, G. Ceballos, R. Rurali and A. Bachtold, *Nat. Nanotechnol.*, 2012, **7**, 301–304.
9 A. K. Naik, M. S. Hanay, W. K. Hiebert, X. L. Feng and M. L. Roukes, *Nat. Nanotechnol.*, 2009, **4**, 445–450.
10 T. P. Burg, M. Godin, S. M. Knudsen, W. Shen, G. Carlson, J. S. Foster, K. Babcock and S. R. Manalis, *Nature*, 2007, **446**, 1066–1069.
11 R. A. Barton, B. Ilic, S. S. Verbridge, B. R. Cipriany, J. M. Parpia and H. G. Craighead, *Nano Lett.*, 2010, **10**, 2058–2063.
12 V. Agache, G. Blanco-Gomez, M. Cochet and P. Caillat, in *2011 IEEE 24th International Conference on Micro Electro Mechanical Systems (MEMS)*, 2011, pp. 157–160.
13 J. Lee, W. Shen, K. Payer, T. P. Burg and S. R. Manalis, *Nano Lett.*, 2010, **10**, 2537–2542.
14 Y. Weng, F. F. Delgado, S. Son, T. P. Burg, S. C. Wasserman and S. R. Manalis, *Lab Chip*, 2011, **11**, 4174.
15 W. H. Grover, A. K. Bryan, M. Diez-Silva, S. Suresh, J. M. Higgins and S. R. Manalis, *Proc. Natl. Acad. Sci. U. S. A.*, 2011, **108**, 10992–10996.
16 S. Son, A. Tzur, Y. Weng, P. Jorgensen, J. Kim, M. W. Kirschner and S. R. Manalis, *Nat. Methods*, 2012, **9**, 910–912.
17 S. M. Knudsen, M. G. Von Muhlen and S. R. Manalis, *Anal. Chem.*, 2012, **84**, 1240–1242.
18 J. L. Arlett and M. L. Roukes, *J. Appl. Phys.*, 2010, **108**, 1–11.
19 E. L. Elson and D. Magde, *Biopolymers*, 1974, **13**, 1–27.
20 B. J. Berne and R. Pecora, *Dynamic Light Scattering: With Applications to Chemistry, Biology, and Physics*, Courier Dover Publications, 2000.
21 K. G. Owens, *Appl. Spectrosc. Rev.*, 1992, **27**, 1–49.
22 L. Van Hove, *Phys. Rev.*, 1954, **95**, 249–262.
23 F. Chiti and C. M. Dobson, *Annu. Rev. Biochem.*, 2006, **75**, 333–366.
24 F. Chiti and C. M. Dobson, *Nat. Chem. Biol.*, 2009, **5**, 15–22.
25 B. Vestergaard, M. Groenning, M. Roessle, J. S. Kastrup, M. Van de Weert, J. M. Flink, S. Frokjaer, M. Gajhede and D. I. Svergun, *PLoS Biol.*, 2007, 5.
26 A. M. Morris, M. A. Watzky and R. G. Finke, *Biochim. Biophys. Acta, Proteins Proteomics*, 2009, **1794**, 375–397.
27 S. E. Bondos, *Curr. Anal. Chem.*, 2006, **2**, 157–170.
28 D. A. White, A. K. Buell, C. M. Dobson, M. E. Welland and T. P. J. Knowles, *FEBS Lett.*, 2009, **583**, 2587–2592.
29 S. Dohn, W. Svendsen, A. Boisen and O. Hansen, *Rev. Sci. Instrum.*, 2007, **78**, 1–3.
30 M. Spiga and G. L. Morini, *Int. Commun. Heat Mass Transfer*, 1994, **21**, 469–475.
31 T. P. Burg, A. R. Mirza, N. Milovic, C. H. Tsau, G. A. Popescu, J. S. Foster and S. R. Manalis, *J. Microelectromech. Syst.*, 2006, **15**, 1466–1476.

32 L. Nielsen, R. Khurana, A. Coats, S. Frokjaer, J. Brange, S. Vyas, V. N. Uversky and A. L. Fink, *Biochemistry*, 2001, **40**, 6036–6046.
33 T. P. Burg, J. E. Sader and S. R. Manalis, *Phys. Rev. Lett.*, 2009, **102**, 228103.
34 B. Swift, P. N. Hawkins, C. Richards and R. Gregory, *Diabetic Med.*, 2002, **19**, 881–882.
35 J. L. Whittingham, D. J. Scott, K. Chance, A. Wilson, J. Finch, J. Brange and G. Guy Dodson, *J. Mol. Biol.*, 2002, **318**, 479–490.
36 F. Librizzi and C. Rischel, *Protein Sci.*, 2005, **14**, 3129–3134.
37 M. R. Nilsson, *Methods*, 2004, **34**, 151–160.
38 M. Biancalana and S. Koide, *Biochim. Biophys. Acta, Proteins Proteomics*, 1804, **2010**, 1405–1412.
39 A. Ahmad, V. N. Uversky, D. Hong and A. L. Fink, *J. Biol. Chem.*, 2005, **280**, 42669–42675.
40 B. O'Nuallain, A. D. Williams, P. Westermark and R. Wetzel, *J. Biol. Chem.*, 2004, **279**, 17490–17499.
41 Y. Ohhashi, M. Kihara, H. Naiki and Y. Goto, *J. Biol. Chem.*, 2005, **280**, 32843–32848.
42 N. Carulla, G. L. Caddy, D. R. Hall, J. Zurdo, M. Gairí, M. Feliz, E. Giralt, C. V. Robinson and C. M. Dobson, *Nature*, 2005, **436**, 554–558.
43 E. Chatani, Y.-H. Lee, H. Yagi, Y. Yoshimura, H. Naiki and Y. Goto, *Proc. Natl. Acad. Sci. U. S. A.*, 2009, **106**, 11119–11124.
44 M. I. Ivanova, S. A. Sievers, M. R. Sawaya, J. S. Wall and D. Eisenberg, *Proc. Natl. Acad. Sci. U. S. A.*, 2009, **106**, 18990–18995.

